Heliyon 10 (2024) e24833

Contents lists available at ScienceDirect

Heliyon

journal homepage: www.cell.com/heliyon

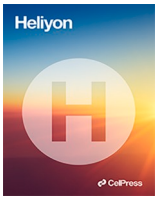

Research article

Dual-targeting CD44 and mucin by hyaluronic acid and 5TR1 aptamer for epirubicin delivery into cancer cells: Synthesis, characterization, *in vitro* and *in vivo* evaluation

Zahra Jamshidi [a,b], Reza Dehghan [a], Mojgan Nejabat [a,**], Khalil Abnous [c], Seyed Mohammad Taghdisi [d,e], Farzin Hadizadeh [f,*]

[a] *Department of Medicinal Chemistry, School of Pharmacy, Mashhad University of Medical Sciences, Mashhad, Iran*
[b] *Student Research Committee, Mashhad University of Medical Sciences, Mashhad, Iran*
[c] *Pharmaceutical Research Center, Pharmaceutical Technology Institute, Mashhad University of Medical Sciences, Mashhad, Iran*
[d] *Targeted Drug Delivery Research Center, Pharmaceutical Technology Institute, Mashhad University of Medical Sciences, Mashhad, Iran*
[e] *Department of Pharmaceutical Biotechnology, School of Pharmacy, Mashhad University of Medical Sciences, Mashhad, Iran*
[f] *Biotechnology Research Institute, Pharmaceutical Technology Institute, Mashhad University of Medical Sciences, Mashhad, Iran*

A R T I C L E I N F O

Keywords:
Breast cancer
Epirubicin
Hyaluronic acid
MUC1
5TR1 aptamer
Targeted drug delivery

A B S T R A C T

One of the revolutionized cancer treatment is active targeting nanomedicines. This study aims to create a dual-targeted drug delivery system for Epirubicin (EPI) to cancer cells. Hyaluronic acid (HA) is the first targeting ligand, and 5TR1 aptamer (5TR1) is the second targeting ligand to guide the dual-targeted drug delivery system to the cancer cells. HA is bound to highly expressed receptors like CD44 on cancer cells. 5TR1, DNA aptamer, is capable of recognizing MUC1 glycoprotein, which is overexpressed in cancer cells.

The process involved binding EPI and 5TR1 to HA using adipic acid dihydrazide (AA) as a linker. The bond between the components was confirmed using ^{1}H NMR. The binding of 5TR1 to HA-AA-EPI was confirmed using gel electrophoresis. The particle size (132.6 ± 9 nm) and Zeta Potential (−29 ± 4.4 mV) were measured for the final nanoformulation (HA-AA-EPI-5TR1). The release of EPI from the HA-AA-EPI-5TR1 nanoformulation was also studied at different pH levels. In the acidic pH (5.4 and 6.5) release pattern of EPI from the HA-AA-EPI-5TR1 nanoformulation was higher than physiological pH (7.4). The cytotoxicity and cellular uptake of the synthetic nanoformula were evaluated using MTT and flow cytometry analysis. Flow cytometry and cellular cytotoxicity studies were exhibited in a negative MUC1^{-}cell line (CHO) and two positive MUC1^{+}cell lines (MCF-7 and C26). Results confirmed that there is a notable contrast between the dual-targeted (HA-AA-EPI-5TR1) and single-targeted (HA-AA-EPI) nanoformulation in MCF-7 and C26 cell lines (MUC1^{+}). *In vivo* studies showed that HA-AA-EPI-5TR1 nanoformulation has improved efficiency with limited side effect in C26 tumor-bearing mice. Also, Fluorescence imaging and pathological evaluation showed reduced side effects in the heart tissue of mice receiving HA-AA-EPI-5TR1 than free EPI.

So, this targeted approach effectively delivers EPI to cancer cells with reduced side effects.

* Corresponding author. Biotechnology Research Center, Pharmaceutical Technology Institute, Mashhad University of Medical Sciences, Mashhad, Iran.
** Corresponding author.
E-mail addresses: nejabatm2@mums.ac.ir (M. Nejabat), hadizadehf@mums.ac.ir (F. Hadizadeh).

https://doi.org/10.1016/j.heliyon.2024.e24833
Received 27 June 2023; Received in revised form 15 January 2024; Accepted 15 January 2024
Available online 17 January 2024

1. Introduction

Epirubicin (EPI), a drug from the anthracycline family, is frequently combined with other anticancer drugs for treating advanced and metastatic breast cancer [1]. It can also be applied in treating other cancers, including non-advanced breast cancer, lung cancer, and colorectal cancer [2]. The most significant side effects of EPI are heart complications and bone marrow suppression. The severity of bone marrow suppression depends on the single dose of EPI, while heart problems, including congestive heart failure, are related to the total amount over time. These factors limit the dose of EPI that can be administered during treatment. By reducing the side effects, the therapeutic window of EPI can be broadened, and its maximum therapeutic capacity can be increased through an increased dose [3,4].

Hyaluronic acid (HA) is a key component of the extracellular matrix and has important roles in cell growth and tissue structure. Because of its biocompatibility, biodegradability, lack of toxicity, hydrophilic nature, and ability to bind drugs through various chemical groups, it is desirable for drug delivery [5–8]. Researchers have utilized HA in drug-delivering nanoparticles and combined with drug-containing liposomes for targeted delivery. HA also interacts with various cell receptors, including intercellular adhesion molecule-1, Toll-like receptor-4, hyaluronic acid receptor for endocytosis, and lymphatic vessel endocytic receptor [9,10]. The CD44 receptor, a membrane-bound glycoprotein, is involved in the activity, attachment, migration, and survival of cancer cells and allows for the internalization of hyaluronic acid. Although normal cells usually have low levels of CD44 expression, cancer cells often have high levels of expression, making HA a useful tool for targeted drug delivery to cancerous tissues [8,11–14].

The 5TR1 aptamer (5TR1) is a specific aptamer that binds to the MUC1 glycoprotein. This glycoprotein is the first of its kind in the mucin family and is found in the membranes of various types of cells, including epithelial cells [15,16]. It express at low levels in the normal cells, while its presence is higher in interstitial and bodily fluids. MUC1 helps maintain the mucus structure on epithelial cells. It has a role in the cell's communication with its environment, responding to changes in pH, salt, osmolarity, and pathogens. However, overexpression of MUC1 has been observed in cancer cells, including breast cancer, where its level has been linked to disease progression and mortality [17–22].

HA and 5TR1 have shown promising results as targeted drug delivery agents in breast cancer.

In this study, the goal is to create a nanoformulation that leverages the capabilities of HA and 5TR1 for effective targeted delivery of EPI. The nanoformula will be evaluated *in vitro* and *in vivo*, and its efficacy will be compared to commercial standard EPI. The other properties of the synthetic nanoformula will also be analyzed through various experiments. Therefore, we replaced the carboxylic acid groups in HA with adipic acid dihydrazide (AA) to create HA-AA. Next, we used the AA linker to connect to EPI, forming HA-AA-EPI by reacting the AA linker's hydrazide with the EPI carbonyl group. Furthermore, the carboxylic acid terminal of the 5TR1 was connected to the hydrazide end of AA to create the final product HA-AA-EPI-5TR1, as illustrated in Fig. 1.

2. Material and methods

2.1. Materials

5TR1 aptamer (5TR1) (5′–COOH–GAAGTGAAAATGACAGAACACAACA-3′) was produced by MicroSynth (Switzerland). Hyaluronic acid (MW = 50,000 Da) (HA) was purchased from Creative PEGworks. The following materials were bought from Sigma-Aldrich

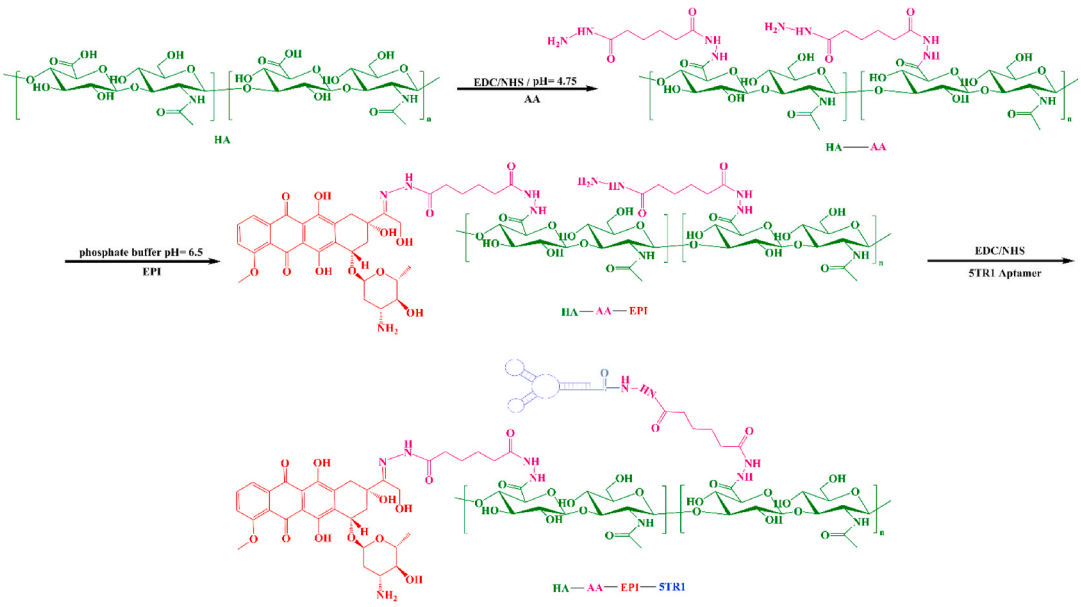

Fig. 1. Synthetic pathway for the HA-AA-EPI-5TR1 conjugate.

in Munich, Germany: N-hydroxysulfosuccinimide (NHS), Adipic acid dihydrazide, 1-ethyl-3-(3-dimethylaminopropyl) carbodiimide hydrochloride (EDC), Epirubicin, and 3-(4,5-dimethylthiazol-2-yl)-2,5-diphenyltetrazolium bromide (MTT). Merck in Darmstadt, Germany, supplied the other necessary materials.

2.2. Cell lines and culture

Human breast adenocarcinoma (MCF-7), Mouse colon adenocarcinoma (C26), and Chinese hamster ovary (CHO) cells were bought from the Pasteur Institute of Iran. All indicated cells were cultured in a medium supplemented with 1 % penicillin-streptomycin and 10 % fetal bovine serum (FBS) in an incubator at 37 °C and a moisturized atmosphere containing 5 % CO_2. Other cell culture materials and supplements were acquired from GIBCO (Darmstadt, Germany).

2.3. Preparation of hyaluronic acid–adipic acid dihydrazide (HA-AA)

HA (12.4 μmol, 5 mg) powder was dissolved in 1 mL of deionized water, and the pH of the solution was adjusted to 4.75 using hydrochloric acid with a concentration of 1 N. Subsequently, NHS (72.1 μmol, 8.3 mg), AA (359.4 μmol, 62.6 mg), and EDC (48 μmol, 9.2 mg) were added to the solution and allowed to react overnight, approximately 24 h and then stop the reaction by the addition of 1 N NaOH [23–26]. The solution was placed in a dialysis bag with a 10,000 Da cut-off and dialyzed for two days against distilled water at room temperature, replacing with the fresh one every 12 h. After dialysis, the solution was removed from the dialysis bag and freeze-dried. The resulting substance was then analyzed using ^{1}H NMR spectroscopy and ^{1}H NMR spectra of A.A and EPI were shown in Figs. S1 and S2.

2.4. Preparation of hyaluronic acid–adipic acid dihydrazide-epirubicin conjugate (HA-AA-EPI)

A solution of HA-AA (4.7 mg) was made by dissolving it in 1 mL of deionized water and adding 1 mL of a pH 6.5 phosphate buffer. Then, 400 μL of EPI (2 mg/ml) was gradually added to the solution while continuously stirring. The reaction was allowed to continue overnight, and the mixture should always be protected against the light [27]. The mixture was transferred to a dialysis bag to purify the product as described above. The purified solution was then freeze dried and analyzed using ^{1}H NMR spectra.

2.5. Loading efficiency and loading content

In this study, loading efficiency and loading content were determined using the following formula, and they were 75 % and 12.5 %, respectively [28,29].

$$\text{Loading efficiency}\% = \frac{\text{amount of the EPI loaded in nanoformulation}}{\text{amount of the initial EPI}} \times 100$$

$$\text{Loading content}\% = \frac{\text{amount of the EPI loaded in nanoformulation}}{\text{amount of final nanoformulation}} \times 100$$

The loading efficiency and loading content of the EPI in the nanoformulation were determined using a fluorescent microplate reader (λ_{Ex} = 480 nm and λ_{Em} = 600 nm) using calibration curve of EPI (0.1–1.5 μg/ml).

2.6. Preparation of hyaluronic acid–adipic acid dihydrazide-epirubicin-5TR1 aptamer conjugate (HA-AA-EPI-5TR1)

5TR1 solution (40 μl, 20 μM), NHS (34.8 μmol, 4 mg), and EDC (28.7 μmol, 5.5 mg) were combined with 1 mL of DNase and RNase-free water. The solution was stirred at 80 rpm at 4 °C for 1 h. The HA-AA-EPI, equivalent to 4.5 mg, was then dissolved in 2 mL of DNase and RNase-free water and added to the first solution, which was then stirred for 24 h at 4 °C while being kept away from the light. The product was purified by centrifuging the solution for 40 min at 10,000 rpm at 4 °C.The upper solution being extracted as the residue and the lower precipitate being the synthetic material. The same steps were repeated using HA-AA to synthesis HA-AA-5TR1.

To evaluate the HA-AA-EPI-5TR1, the precipitate was dissolved in 1 ml of DNase and RNase-free water. The 5TR1 standard solution was diluted to 375 μl with DNase and RNase-free water. 8 μl each of diluted 5TR1 standard solution, synthetic HA-AA-EPI-5TR1 solution, and the residue solution from the HA-AA-EPI-5TR1 reaction were mixed with 2 μl of Dye gel and loaded into separate wells of a 2 % agarose gel in TBE buffer (pH = 8.3). The gel was subjected to an electric current of 100 mV for 20 min at room temperature, and the UV absorption of the gel was evaluated using a Gel Doc (Alliance 4.7, UK). The same experiment was repeated for the synthetic HA-AA-5TR1 sample.

2.7. Particle size determination

0.2 mg of the sample was dissolved in 1 mL of deionized water. The nanoformula's surface charge and particle size distribution were analyzed using dynamic light scattering (DLS) by the Zeta Sizer instrument (NANO-ZS, from Malvern, UK).

2.8. In vitro evaluation of EPI release

A test was performed to determine the emission of 1 ml solutions of HA-AA-EPI-5TR1. These solutions were placed in separate dialysis bags with a cut-off of 10,000 Da and immersed in 45 ml of citrate buffer (pH 5.4) or phosphate buffer (pH 7.4 and 6.5). The bags were then kept in a shaker incubator at 37 °C and rotated at 50 rpm. 1 mL of external medium was taken from each environment (PBS or citrate buffer) at different intervals (0, 2, 4, 6, 8, 10, 12, 24 and 48 h) and exchanged with 1 mL of fresh citrate buffer or PBS. The fluorescence was measured by a fluorescence reader (BioTeK, USA) at ($\lambda_{Ex} = 480$ nm, $\lambda_{Em} = 600$ nm).

2.9. In vitro cytotoxicity study

The toxicity of EPI, HA-AA-EPI, HA-AA-EPI-5TR1, HA-AA, and HA-AA-5TR1 was assessed using the MTT test. The IC_{50} of EPI was calculated to be 1.8 μg/mL, 2.5 μg/mL, and 1.4 μg/mL for the CHO, MCF-7, and C26 cell lines, respectively. The cell lines were seeded in a 96-well microplate, with 5000 cells in each well, and incubated for 24 h. Then all prepared nanoformulations EPI, HA-AA-EPI, HA-AA-EPI-5TR1, HA-AA, and HA-AA-5TR1 were transferred to wells (n = 3) for 3 h. The medium was replaced after 3 h, and 48 h later, for cytotoxicity measurement, 20 μL MTT stock solution (5 mg/mL) was transferred per well for another 3 h. Then, the solution was aspirated and the addition of DMSO 100 μL to the wells. The absorbance of each well was calculated at 570 nm and 630 nm by an Infinite® 200 PRO multimode microplate reader.

2.10. Cellular uptake evaluation by flow cytometry

In this study, 15×10^4 cells from each CHO, C26, and MCF-7 cell line were placed into individual wells of a 24-well plate. The plate was kept in an incubator for 24 h at 37 °C and with a 5 % CO_2 atmosphere. The cell lines were exposed to EPI and HA-AA-EPI-5TR1 concentrations of 1.8 μg/ml, 2.5 g/ml, and 1.4 μg/ml for 4 h. After 4 h, the contents of each well were drained, and trypsin was added. The wells were then filled with fresh medium and centrifuged (1500 rpm, 5 min). The supernatant was removed and re-suspended cells in PBS. Finally, the cell suspensions were analyzed using flow cytometry in the FL2 channel.

2.11. Therapeutic efficacy in vivo

To establish tumor therapy models, 5–6 weeks-old female BALB/c mice (18–22 g) were anesthetized using ketamine/xylazine through intraperitoneal injection. 3×10^5 of the C26 cells were implanted subcutaneously in the mice and randomly divided into four groups (n = 4). After the tumor size reached about ~15 mm^3, EPI, HA-AA-EPI, and HA-AA-EPI-5TR1 (containing 2 mg/kg EPI) were injected (IV) into the tail vein, and the control mice received 100 μL PBS. The mice were weighed, and the tumor sizes were measured periodically for 28 days post-injection. Tumor volume was calculated by applying the formula volume = abc/2. The toxicity of each treatment was determined by monitoring survival rates and body weight. When the tumors reached more than 1.5 cm in any dimension or had a weight loss of over 20 % of the initial weight, the mice were sacrificed. All animal studies in this experiment were approved by the ethical research committee of Mashhad University of Medical Sciences (IR.MUMS.AEC.1401.020).

2.12. Ex vivo fluorescence imaging

10-days after C26-tumor inoculation, the tumor size reached about 200 mm^3. The mice randomly assigned to two groups (3 mice per group), and treated by the HA-AA-EPI-5TR1 nanoformulation and EPI (2 mg EPI equiv/kg) via the tail vein. The mice were sacrificed after 24 h post-injection. Mouse's heart, liver, tumor, spleen, lung and kidney were collected and fluorescence images were captured at 450 and 600 nm using the KODAK IS imaging system.

2.13. Pathological evaluation

28-day post-injection of the first dose of the synthesized nanoformulations, mice were sacrificed, and liver tumor and heart were isolated. Tissue samples were fixed in formalin, then sectioned into slices at a thickness of 5 μm. The ready tissue samples were stained with hematoxylin and eosin. Images were captured using a light microscope Olympus IX70.

2.14. Statistical analysis

One-way ANOVA was used for statistical analysis. The results were considered statistically significant if the p-value was less than or equal to 0.05, 0.01, 0.001, or 0.0001, indicated by asterisks (*) in the results. The significance level was denoted as *$p \leq 0.05$, **$p \leq 0.01$, ***$p \leq 0.001$, and ****$p \leq 0.0001$.

3. Results

3.1. Spectral studies

The ^{1}H NMR spectrum of HA, HA-AA and HA-AA-EPI were shown in Fig. 2. The ^{1}H NMR spectrum reveals a ratio between the

integral of peaks at 2.2–2.4 ppm, which is attributed to the CH_2CH_2 of the AA, and the integral of peak at 1.9 ppm related to the $NHCOCH_3$ of HA, indicating a 25 % and substitution of HA with the AA [25–27,30–32]. Furthermore, the ratio between the integral peaks at 7.4–7.6 ppm, which corresponds to the C–H $_{aromatic}$ of EPI, and the integral of the peak at 1.9 ppm related to the $NHCOCH_3$ of HA shows 2.5 % of carboxylic acid substitution of HA with EPI.

3.2. Physicochemical properties

The particle size of pure HA was measured to be 112 ± 4.0 nm with a zeta potential of −23.3 ± 2.3 mV and a polydispersity index of 0.212. The particle size of the HA-AA-EPI sample to be 107 ± 8.1 nm with a zeta potential of −26.7 ± 3.4 mV and a polydispersity index of 0.287. Also, the particle size of the HA-AA-EPI-5TR1 sample was determined by DLS to be 132.6 ± 9.3 nm a zeta potential of −29 ± 4.4 mV with polydispersity index of 0.192, as indicated in Table 1. The DLS results showed that the synthetic nanoformulations had a particle size below 200 nm. Regarding the results of the polydispersity index, it could be said that these particles have good homogeneity in size. Zeta potential suggested relatively good stability of particles.

This particle size offered the likelihood of intravenous injection of the formula into the animal. Also, it made the EPR (enhanced permeability and retention) phenomenon possible for the targeted delivery of EPI to the cancer tissue. The EPR effect refers to the ability of certain particle systems to selectively accumulate in tumors due to their increased vascular permeability compared to normal tissues, thereby allowing for the targeted delivery of drugs to cancerous tissues [33].

3.3. Characterization of 5TR1 conjugation

The results of the UV absorption of HA-AA-EPI-5TR1 gel electrophoresis were depicted in Fig. 3. The wells in the image contained the HA-AA-EPI-5TR1 (synthetic sample), the 5TR1 (standard aptamer), and the reaction supernatant. A band with a higher molecular

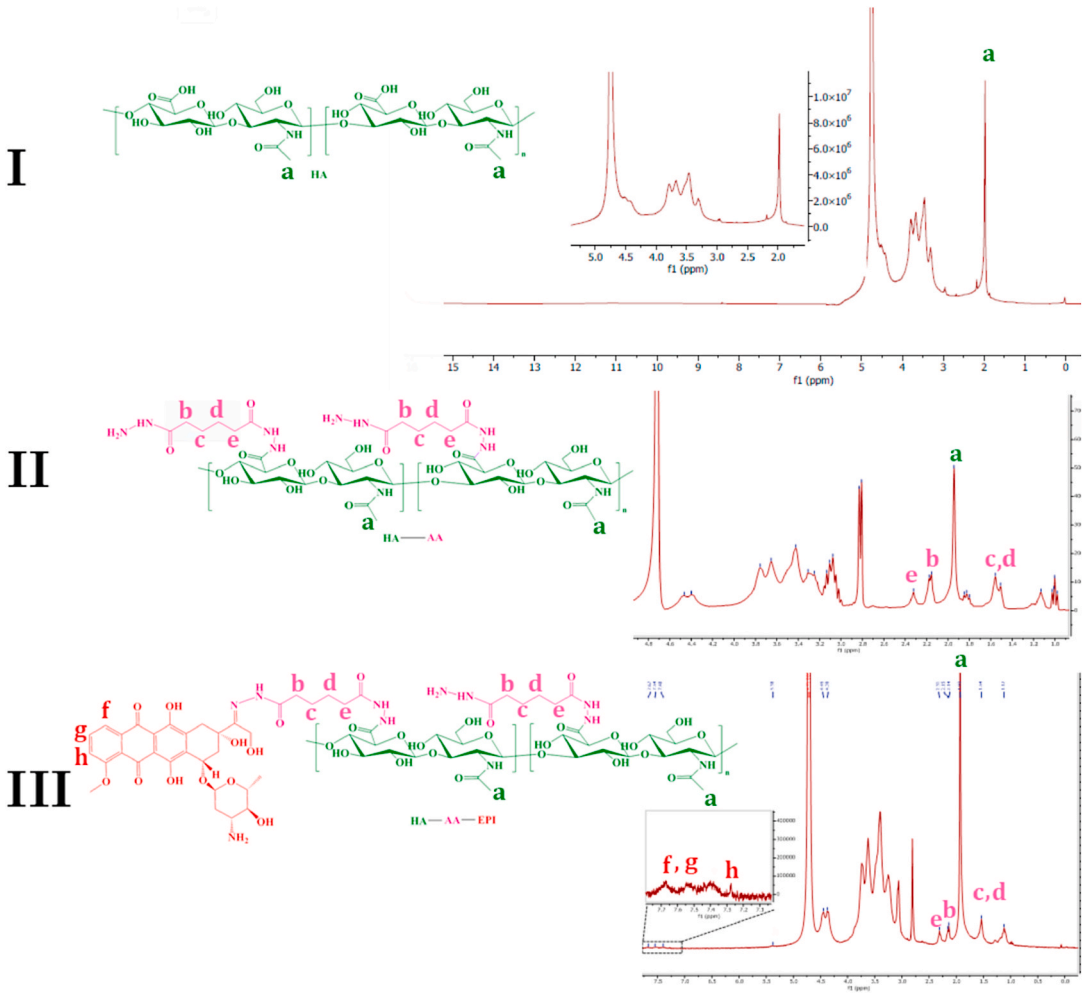

Fig. 2. ^{1}H NMR spectrum of **I:** HA, **II:** HA-AA and, **III:** HA-AA-EPI in D_2O (300 MHz).

Table 1
Characteristics of particles.

Sample	Particle Size (nm)	Zeta Potential (mV)	Polydispersity Index
HA	**112 ± 4.0**	**−23.3 ± 2.3**	**0.212**
HA-AA-EPI	**107 ± 8.1**	**−26.7 ± 3.4**	**0.287**
HA-AA-EPI-5TR1	**132.6 ± 9.3**	**−29 ± 4.4**	**0.192**

Data were presented as means ± SD, n = 3.

weight region in the image was a sign of the binding of 5TR1 to the modified HA-AA-EPI. The absence of a band in the supernatant suggested the lack of additional 5TR1 in the reaction supernatant and again reconfirmed conjugation.

3.4. EPI release studies

The release of EPI from HA-AD-EPI-5TR1 was studied *in vitro* in three different pH conditions: citrate buffer at pH 5.4 and phosphate buffer at pH 7.4 and 6.5. The results are depicted in Fig. 4.

Based on the results, the release of EPI from HA-AA-EPI-5TR1 reaches the limit in the first 5–10 h. The release of EPI was significantly higher at a more acidic pH of 6.5 and 5.4, compared to pH 7.4. The acidic pH of tumors can often be lower than the surrounding healthy tissue, making it a unique target for pH-sensitive drug delivery systems. The hydrazone bond between EPI and the carrier (AA) is susceptible to acidic conditions. According to the results of drug release in an acidic environment such as cancer tissue, more EPI can be released, leading to a change in the concentration of the drug from healthy tissue to cancerous tissue. By increasing the release of the drug at these lower pH (5.4 and 6.5 (, the targeted delivery system can effectively deliver higher concentrations of the drug to the tumor site, potentially improving treatment efficacy.

3.5. Cytotoxicity evaluation

The viability of cells treated with EPI, HA-AA-EPI, HA-AA-EPI-5TR1, HA-AA and HA-AA-5TR1 is depicted in Fig. 5.

The results of the MTT cytotoxicity test indicated that HA-AA and HA-AA-5TR1 did not cause significant toxicity in CHO, MCF-7, and C26 cell lines, thereby confirming the biocompatibility of the carrier. On the other hand, the results showed that the HA-AA-EPI and HA-AA-EPI-5TR1 were more toxic than free EPI in the MCF-7 and C26 cell lines. It showed the major function of 5TR1 and HA in targeted delivery to the cancer cells by MUC1 and CD44 receptor [9,21,34–38]. Studies have shown that the interaction of HA with CD44 on the surface of cancer cells can lead to the internalization of HA-CD44 complexes, which can be used to deliver therapeutic agents directly to cancer cells [38–40]. Additionally, some studies have suggested that the interaction of HA with CD44 on the surface of cancer cells can induce apoptosis, or cell death, thereby providing an additional mechanism for cancer cell killing. MUC1 is a protein overexpressed on the surface of various cancer cells, including breast cancer. By binding specifically to MUC1 on the surface of cancer cells, the 5TR1 can be used as a targeting moiety to deliver therapeutic agents directly to cancer cells, thereby increasing the specificity and efficacy of cancer therapies. CHO cells are commonly used as control cells in studies of cancer cell biology because they are negative for both CD44 and MUC1 expression. Hence ineffectiveness of nanoformulations on the CHO provided evidence that the HA-AA-EPI-5TR1 conjugates were selectively targeting MUC1 and CD44. The HA-AA-EPI-5TR1 was found to be more toxic on the MCF7 and C26 cell lines compared to HA-AA-EPI. This suggested that adding the 5TR1 to the HA-AA-EPI increased the toxicity of the nanoformulation to these cell lines.

3.6. Flow cytometry evaluation

Fig. 6 represents the results of flow cytometry analysis and compares the uptake of EPI and HA-AA-EPI-5TR1 into the CHO, MCF-7, and C26 cells. The histograms, which display the fluorescence intensity values on a logarithmic scale, indicate the fluorescence intensity of cells in each group on the FL2 channel.

The cellular uptake of EPI in the targeted nanoformulation HA-AA-EPI-5TR1 was higher than that of EPI in the cell lines MCF-7 and C26. However, this result was not observed in the CHO cell line, which lacks CD44 and MUC1 targets, and the cellular internalization of the targeted nanoformulation and EPI was equal. This was in agreement with cytotoxicity results (as shown in Fig. 5).

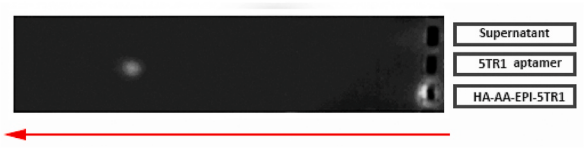

Fig. 3. Gel electrophoresis depiction for HA-AA-EPI-5TR1, 5TR1 aptamer, and supernatant.

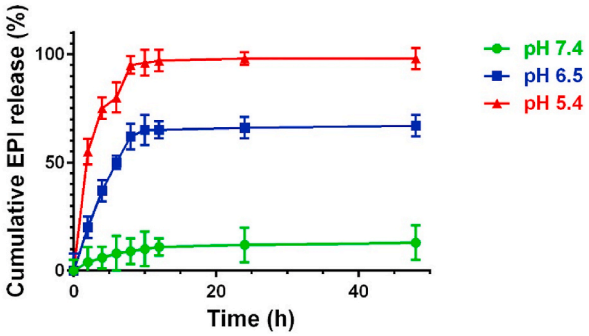

Fig. 4. The EPI release pattern from HA-AA-EPI-5TR1 in phosphate buffer (pH 6.5 and pH 7.4) and citrate buffer (pH 5.4) (n = 3).

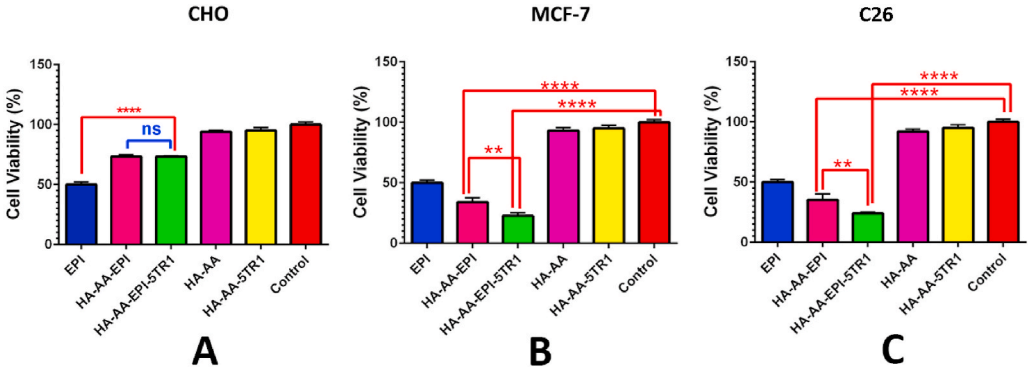

Fig. 5. The *in vitro* cytotoxicity of **A:** CHO, **B:** MCF-7 and, **C:** C26 cell lines incubated with free EPI, HA-AA-EPI, HA-AA-EPI-5TR1, HA-AA and HA-AA-5TR1 (n = 3), ns, **p ≤ 0.01, ****p ≤ 0.0001.

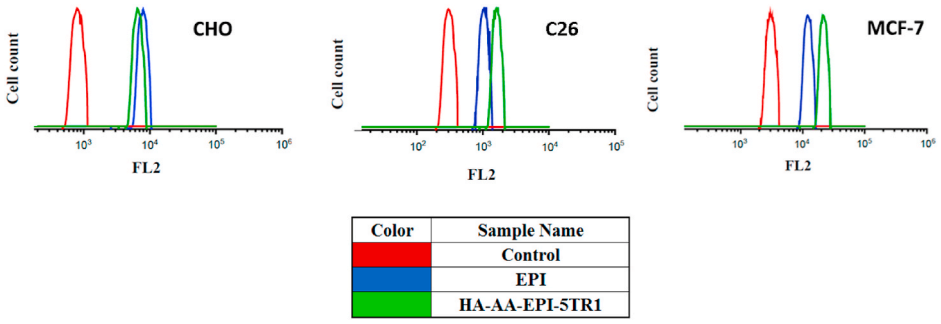

Fig. 6. Flow cytometry analysis of C26, MCF-7 and CHO cell lines treated with HA-AA-EPI-5TR1 and EPI (n = 3).

3.7. Ex vivo fluorescence analysis

Tumor accumulation and biodistribution of HA-AA-EPI-5TR1 and EPI were evaluated 24 h post-administration by the fluorescence system, and KODAK IS *in vivo* imaging. As shown in Fig. 7A, HA-AA-EPI-5TR1 showed greater EPI accumulation than free EPI in the tumor site. Also, as shown in Fig. 7A, less fluorescence was observed in the heart tissue of mice treated with HA-AA-EPI-5TR1 compared to free EPI. Then, each mouse's region of interest (ROI) investigation was done for heart, liver, tumor, spleen, lung, and kidney tissue by applying KODAK Molecular Imaging software 5.0. Additionally, the obtained results showed that there is a notable change in fluorescence intensity in the tumor site of the mice which free EPI injected in comparison with HA-AA-EPI-5TR1. Heart tissue of mice after receiving HA-AA-EPI-5TR1 showed a lower intensity of fluorescence compared whit free EPI (Fig. 7B).

3.8. In vivo antitumor effects

Weight of mice showed no notable modification between all of the groups (Fig. 8A). The survival rate analysis displayed that 25 %

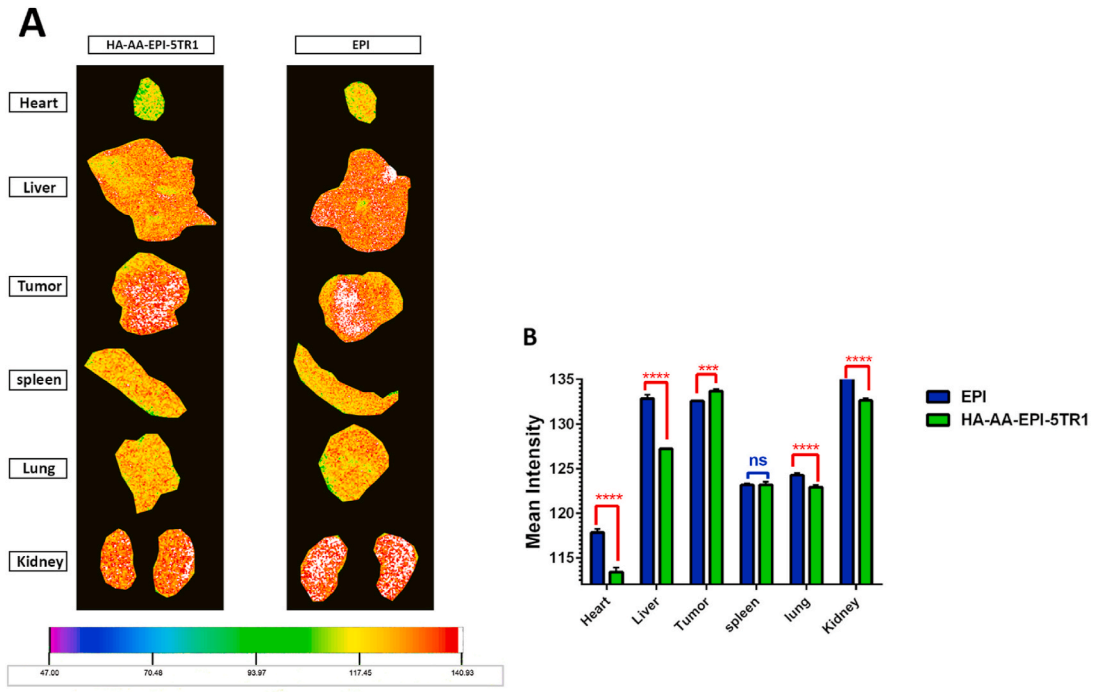

Fig. 7. **A**: The *ex vivo* fluorescence images of the heart, liver, tumor, spleen, lung and kidney post-administration of EPI, HA-AA-EPI-5TR1, **B**: The ROI analysis of the EPI fluorescence in the heart, liver, tumor, spleen, lung and kidney tissue post-administration (n = 3). ns $p \geq 0.05$, ***$p \leq 0.001$, ****$p \leq 0.0001$.

of mice treated with free EPI died within 22 days post-administration, although in the group received with HA-AA-EPI-5TR1 remained alive until day 28 (Fig. 8B). Also, HA-AA-EPI-5TR1 could remarkably decrease tumor growth compared with other formulations (Fig. 8C).

3.9. Pathological study

Twenty-eight days after receiving synthesized nanoformulations, the organ toxicity was examined. Large necrotic regions were observed in tumor specimens of mice that received HA-AA-EPI-5TR1 in contrast with those treated with HA-AA-EPI. As shown in Fig. 9, there was no histopathological modification in the liver tissue of mice treated with HA-AA-EPI-5TR1.

In the heart tissue of the EPI-treated group, the observed pathological cell injury could be considered a serious side effect of EPI. This was not observed in other groups.

4. Discussion

In vitro release patterns of EPI from HA-AA-EPI-5TR1 nanoformulation as a function of time at three different pH (5.4, 6.5 and 7.4) were presented in Fig. 4. The results displayed that the HA-AA-EPI-5TR1 nanoformulation was stable under physiological condition (pH 7.4), although could release drugs in the acidic microenvironment of cancer cells (pH 5.4). The findings showed the utility of pH-sensitive hydrazone bond in the structure of HA-AA-EPI-5TR1 nanoformulation to effectively release EPI in the acidic pH of cancer cells. Recently reported Dual-targeted HA-Doxorubicin (Dox) formula showed similar behavior [9,23,41–43]. Tang et al. has reviewed pH-sensitive polymers in pharmaceutics [44,45].

Compared to free EPI, two other nanoformulations (HA-AA-EPI-5TR1, HA-AA-EPI) demonstrated higher cytotoxicity in both C26 and MCF-7 cells (Fig. 5). The cytotoxicity of HA-AA-EPI-5TR1 nanoformulation on C26 and MCF-7 cells was stronger than that of HA-AA-EPI nanoformulation because 5TR1 targets MUC1 receptors. In previous work 5TR1 was used for targeted delivery of Dox and Smac peptide [13,21]. To explore the cellular uptake of HA-AA-EPI-5TR1 versus EPI, cellular uptake studies were performed on C26, MCF-7, and CHO cells as MUC^{+} and MUC^{-} cells, respectively, using flow cytometry (Fig. 6). The cellular uptake of the targeted (HA-AA-EPI-5TR1 and HA-AA-EPI) and non-targeted (EPI) nanoformulation by CHO cells was identical. The obtained results displayed a higher uptake of the HA-AA-EPI-5TR1 (dual-targeted) by MCF-7 and C26 cells compared to that of EPI (non-targeted) [46,47].

The tumor volume of C26-tumor-bearing mice received with PBS (control group) elevated quickly, and the groups treated by HA-AA-EPI-5TR1 nanoformulations demonstrated suppression of tumor growth (Fig. 8C). One targeted (HA-AA-EPI-5TR1), and two targeted (HA-AA-EPI-5TR1) nanoformulations exhibited higher antitumor effect compared to free EPI. Increasing accumulation of EPI in tumors by targeting agents (HA and 5TR1) (Fig. 8C).

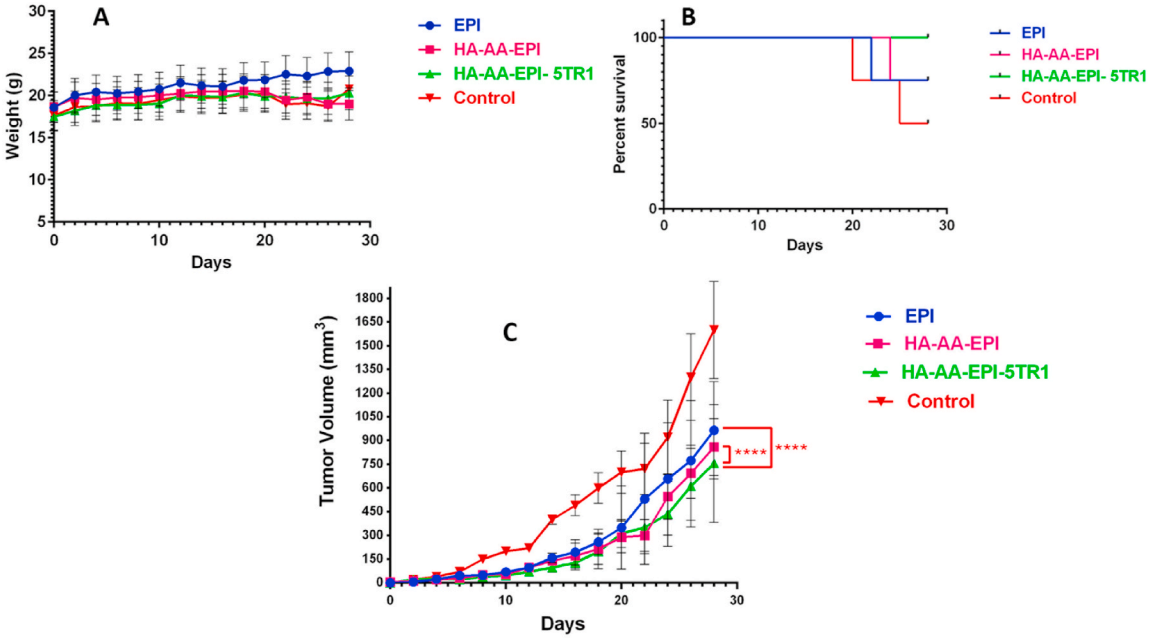

Fig. 8. *In vivo* antitumor effects of the EPI, HA-AA-EPI, HA-AA-EPI-5TR1 injected to C26-tumor-bearing mice (n = 4) (EPI 5 mg/kg) bodyweight (A), survival rates (B), and tumor volume changes (C).

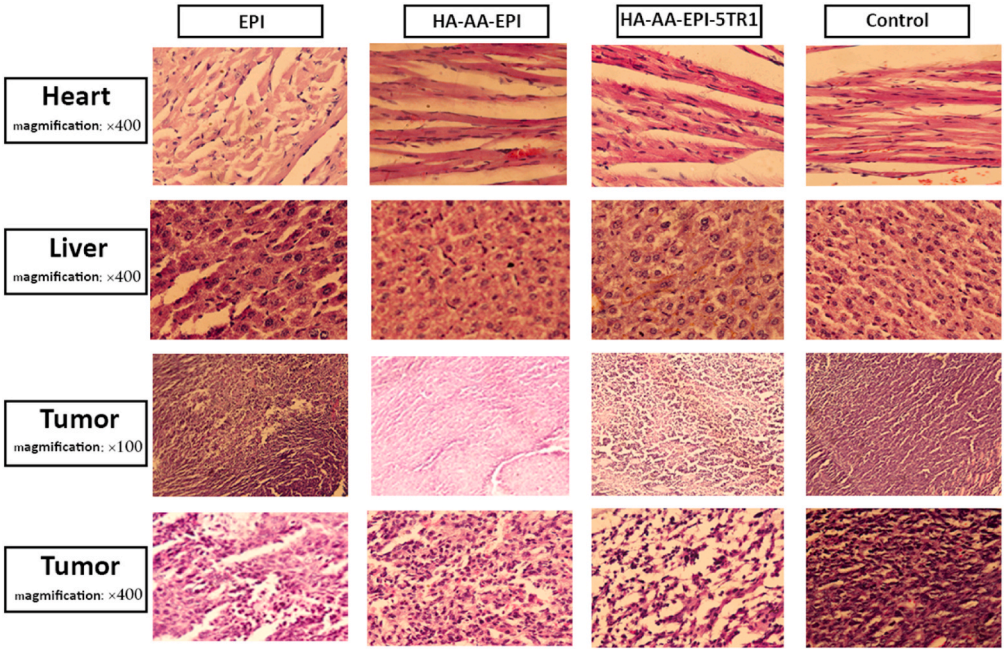

Fig. 9. (H&E) stained heart, liver and tumor tissues 28 days post-injection of EPI, HA-AA-EPI, HA-AA-EPI-5TR1 in C26-tumorized mice.

Various treatment groups revealed no significant body weight loss, as seen in Fig. 8A. Histopathological examinations revealed a large necrotic region in the tumor tissue of mice that received HA-AA-EPI-5TR1 compared to those that received HA-AA-EPI. HA-AA-EPI-5TR1 showed significant tumor inhibition compared to other treatment groups. Similarly, Dox- PLGA-PEG-polymerosomes showed selective tumor inhibition activity compared to free Dox [48]. This confirmed the significance of both 5TR1 and HA as targeting agents for selective nanoformulation delivery into tumor site. This result illustrated the tumor penetration capability of HA-AA-EPI-5TR1 due to both the HA and 5TR1 targeting effect (Fig. 9). Biodistribution of the HA-AA-EPI-5TR1 and EPI systems was evaluated in C26 tumor-bearing mice. Also, in the tumor tissue, maximum accumulation of targeted HA-AA-EPI-5TR1 was observed

(Fig. 7B). As it was depicted in Fig. 7A, ROI examination showed the notably lower intensity of fluorescent was detected in the heart tissue of mice that received the targeted nanoformulation (Fig. 7A).The polymerosomes loaded with Gadmium as MRI imaging and Dox showed similar tissue distribution [49].

5. Conclusion

In this work, we constructed a drug delivery system for EPI with two targetings (HA and 5TR1) and controlled release (hydrazone bonds) characteristics to decrease the systemic cytotoxicity of chemotherapeutics. EPI was chemically conjugated to the polymer via hydrazone bonds, which effectively prevented premature EPI release in the blood circulation and achieved prompt intracellular release in an acidic microenvironment. A dual-targeting drug delivery system (HA-AA-EPI-5TR1) showed antitumor efficacies while significantly reducing the systemic toxicity of EPI. 5TR1 importantly prompted the targeting ability of drug delivery systems for guided transportation to colorectal cancer cells. Dual-targeted nanoformulation (HA-AA-EPI-5TR1) nanoformulations significantly suppressed tumor growth rate in C26 tumor-bearing mice. These data strongly proposed that the prepared dual-targeted nanoformula with targeting capability, effective and non-toxic, could be considered a hopeful candidate for the development of an innovative system.

Data availability statement

The authors declare the data is included in the article and no additional data is available.

CRediT authorship contribution statement

Zahra Jamshidi: Writing – review & editing, Writing – original draft, Visualization, Methodology, Investigation, Formal analysis, Data curation. **Reza Dehghan:** Visualization, Validation, Methodology, Investigation, Formal analysis, Data curation. **Mojgan Nejabat:** Writing – review & editing, Writing – original draft, Project administration, Methodology, Conceptualization. **Khalil Abnous:** Writing – original draft, Visualization, Project administration, Investigation. **Seyed Mohammad Taghdisi:** Writing – review & editing, Validation, Project administration, Methodology. **Farzin Hadizadeh:** Writing – review & editing, Visualization, Supervision, Project administration, Funding acquisition, Conceptualization.

Declaration of competing interest

The authors declare that they have no known competing financial interests or personal relationships that could have appeared to influence the work reported in this paper.

Acknowledgment

This project was supported by Mashhad University of Medical Sciences (grant no 4010289).

Appendix A. Supplementary data

Supplementary data to this article can be found online at https://doi.org/10.1016/j.heliyon.2024.e24833.

References

[1] M. Untch, F. von Koch, S. Kahlert, G. Konecny, Overview of epirubicin-based adjuvant therapy in breast cancer, Clin. Breast Cancer 1 (Suppl 1) (2000) S41–S45.
[2] G.L. Plosker, D.J.D. Faulds, Epirubicin: a review of its pharmacodynamic and pharmacokinetic properties, and therapeutic use in cancer chemotherapy, Drugs 45 (5) (1993) 788–856.
[3] D. Ormrod, K. Holm, K. Goa, C.J.D. Spencer, aging. Epirubicin: a review of its efficacy as adjuvant therapy and in the treatment of metastatic disease in breast cancer, Drugs 15 (1999) 389–416.
[4] R.J. Cersosimo, W. Hong, Epirubicin: a review of the pharmacology, clinical activity, and adverse effects of an adriamycin analogue, J. Clin. Oncol. 4 (3) (1986) 425–439.
[5] C.P. Fu, X.Y. Cai, S.L. Chen, H.W. Yu, Y. Fang, X.C. Feng, et al., Hyaluronic acid-based nanocarriers for anticancer drug delivery, Polymers 15 (10) (2023).
[6] Y. Jia, S. Chen, C. Wang, T. Sun, L. Yang, Hyaluronic acid-based nano drug delivery systems for breast cancer treatment: recent advances, Front. Bioeng. Biotechnol. 10 (2022) 990145.
[7] N. Salari, K. Mansouri, E. Valipour, F. Abam, M. Jaymand, S. Rasoulpoor, et al., Hyaluronic acid-based drug nanocarriers as a novel drug delivery system for cancer chemotherapy: a systematic review, Daru : journal of Faculty of Pharmacy, Tehran University of Medical Sciences 29 (2) (2021) 439–447.
[8] G. Huang, H. Huang, Hyaluronic acid-based biopharmaceutical delivery and tumor-targeted drug delivery system, J. Contr. Release 278 (2018) 122–126.
[9] Z. Jamshidi, T.S. Zavvar, M. Ramezani, M. Alibolandi, F. Hadizadeh, K. Abnous, et al., Dual-targeted and controlled release delivery of doxorubicin to breast adenocarcinoma: in vitro and in vivo studies, Int. J. Pharm. 623 (2022) 121892.
[10] M. Mirzaee, S. Semnani, G. Roshandel, M. Nejabat, Z. Hesari, H. Joshaghani, Strontium and antimony serum levels in healthy individuals living in high-and low-risk areas of esophageal cancer 34 (7) (2020) e23269.
[11] S. Arpicco, P. Milla, B. Stella, F.J.M. Dosio, Hyaluronic acid conjugates as vectors for the active targeting of drugs, genes and nanocomposites in cancer treatment, Molecules 19 (3) (2014) 3193–3230.
[12] J. Necas, L. Bartosikova, P. Brauner, J. Kolar, Hyaluronic acid (hyaluronan): a review, Vet. Med. 53 (8) (2008) 397–411.

[13] M. Nejabat, F. Soltani, M. Alibolandi, M. Nejabat, K. Abnous, F. Hadizadeh, et al., Smac peptide and doxorubicin-encapsulated nanoparticles: design, preparation, computational molecular approach and in vitro studies on cancer cells, J. Biomol. Struct. Dynam. 40 (2) (2022) 807–819.
[14] H. Joshaghani, H-s Mirkarimi, S. Besharat, G. Roshandel, O. Sanaei, M. Nejabat, Comparison of the serum levels of trace elements in areas with high or low rate of esophageal cancer, Middle East Journal of Digestive Diseases 9 (2) (2017) 81.
[15] A. Biabangard, A. Asoodeh, M.R. Jaafari, M. Mashreghi, Study of FA12 peptide-modified PEGylated liposomal doxorubicin (PLD) as an effective ligand to target Muc1 in mice bearing C26 colon carcinoma: in silico, in vitro, and in vivo study, Expet Opin. Drug Deliv. 19 (12) (2022) 1710–1724.
[16] S.A. Moosavian, K. Abnous, J. Akhtari, L. Arabi, A. Gholamzade Dewin, M. Jafari, 5TR1 aptamer-PEGylated liposomal doxorubicin enhances cellular uptake and suppresses tumour growth by targeting MUC1 on the surface of cancer cells, Artif. Cell Nanomed. Biotechnol. 46 (8) (2018) 2054–2065.
[17] Gendler Sjjjomgb, neoplasia. MUC1, the renaissance molecule, Journal of mammary gland biology 6 (2001) 339–353.
[18] J.F. Lee, G.M. Stovall, Ellington Adjcoicb, Aptamer therapeutics advance, Curr. Opin. Chem. Biol. 10 (3) (2006) 282–289.
[19] B.J. Hicke, A.W. Stephens, T. Gould, Y.-F. Chang, C.K. Lynott, J. Heil, et al., Tumor targeting by an aptamer, J. Nucl. Med. 47 (4) (2006) 668–678.
[20] M.S. Nabavinia, A. Gholoobi, F. Charbgoo, M. Nabavinia, M. Ramezani, K.J.M.R.R. Abnous, Anti-MUC1 aptamer: a potential opportunity for cancer treatment, Med. Res. Rev. 37 (6) (2017) 1518–1539.
[21] M. Nejabat, F. Eisvand, F. Soltani, M. Alibolandi, S.M. Taghdisi, K. Abnous, et al., Combination therapy using Smac peptide and doxorubicin-encapsulated MUC 1-targeted polymeric nanoparticles to sensitize cancer cells to chemotherapy: an in vitro and in vivo study, Int. J. Pharm. 587 (2020) 119650.
[22] T. Rezaei, K. Sadri, M. Nejabat, R. Sadeghi, F. Hadizadeh, Preparation and biomolecule conjugation of [99 mTc] Tc-MAG3, Iran. J. Nucl. Med. 31 (1) (2023) 70–78.
[23] A. Malfanti, G. Catania, Q. Degros, M. Wang, M. Bausart, V.J.P. Préat, Design of bio-responsive hyaluronic acid–doxorubicin conjugates for the local treatment of glioblastoma, Pharmaceutics 14 (1) (2022) 124.
[24] Y. Luo, K.R. Kirker, G.D. Prestwich, Cross-linked hyaluronic acid hydrogel films: new biomaterials for drug delivery, J. Contr. Release : official journal of the Controlled Release Society 69 (1) (2000) 169–184.
[25] J.W. Kuo, D.A. Swann, G.D. Prestwich, Chemical modification of hyaluronic acid by carbodiimides, Bioconjugate Chem. 2 (4) (1991) 232–241.
[26] D.R. Vogus, M.A. Evans, A. Pusuluri, A. Barajas, M. Zhang, V. Krishnan, et al., A hyaluronic acid conjugate engineered to synergistically and sequentially deliver gemcitabine and doxorubicin to treat triple negative breast cancer, J. Contr. Release 267 (2017) 191–202.
[27] S. Cai, S. Thati, T.R. Bagby, H.-M. Diab, N.M. Davies, M.S. Cohen, et al., Localized doxorubicin chemotherapy with a biopolymeric nanocarrier improves survival and reduces toxicity in xenografts of human breast cancer, J. Contr. Release 146 (2) (2010) 212–218.
[28] C. Fu, R.-M. Yang, L. Wang, N-n Li, M. Qi, X-d Xu, et al., Surface functionalization of superparamagnetic nanoparticles by an acid-liable polysaccharide-based prodrug for combinatorial monitoring and chemotherapy of hepatocellular carcinoma, RSC Adv. 7 (66) (2017) 41919–41928.
[29] H. Onishi, A. Fukasawa, A. Miatmoko, K. Kawano, Y. Ikeuchi-Takahashi, Y. Hattori, Preparation of chondroitin sulfate-adipic acid dihydrazide-doxorubicin conjugate and its antitumour characteristics against LLC cells, J. Drug Target. 25 (8) (2017) 747–753.
[30] T. Pouyani, G.D. Prestwich, Functionalized derivatives of hyaluronic acid oligosaccharides: drug carriers and novel biomaterials, Bioconjugate Chem. 5 (4) (1994) 339–347.
[31] Y. Yin, C. Fu, M. Li, X. Li, M. Wang, L. He, et al., A pH-sensitive hyaluronic acid prodrug modified with lactoferrin for glioma dual-targeted treatment, Mater. Sci. 67 (2016) 159–169.
[32] A. Charlot, A. Heyraud, P. Guenot, M. Rinaudo, R.J.B. Auzély-Velty, Controlled synthesis and inclusion ability of a hyaluronic acid derivative bearing β-cyclodextrin molecules, Biomacromolecules 7 (3) (2006) 907–913.
[33] J. Sandoval, J. Ventura-Sobrevilla, D. Boone-Villa, R. Ramos-González, M. Velázquez, Y. Silva-Belmares, et al., Carbon Nanomaterials as Pharmaceutic Forms for Sustained and Controlled Delivery Systems. Nanomaterials for Drug Delivery and Therapy, Elsevier, 2019, pp. 403–434.
[34] H.J. Jhan, J.J. Liu, Y.C. Chen, D.Z. Liu, M.T. Sheu, H.O. Ho, Novel injectable thermosensitive hydrogels for delivering hyaluronic acid-doxorubicin nanocomplexes to locally treat tumors, Nanomedicine (London, England) 10 (8) (2015) 1263–1274.
[35] A. Bahreyni, M. Alibolandi, M. Ramezani, A. Sarafan Sadeghi, K. Abnous, S.M. Taghdisi, A novel MUC1 aptamer-modified PLGA-epirubicin-PβAE-antimir-21 nanocomplex platform for targeted co-delivery of anticancer agents in vitro and in vivo, Colloids and surfaces B, Biointerfaces. 175 (2019) 231–238.
[36] Y. Hu, J. Duan, Q. Zhan, F. Wang, X. Lu, X.D. Yang, Novel MUC1 aptamer selectively delivers cytotoxic agent to cancer cells in vitro, PLoS One 7 (2) (2012) e31970.
[37] K.K. Vangara, J.L. Liu, S. Palakurthi, Hyaluronic acid-decorated PLGA-PEG nanoparticles for targeted delivery of SN-38 to ovarian cancer, Anticancer research 33 (6) (2013) 2425–2434.
[38] P. Kesharwani, R. Chadar, A. Sheikh, W.Y. Rizg, A.Y. Safhi, CD44-Targeted nanocarrier for cancer therapy, Front. Pharmacol. 12 (2021) 800481.
[39] G. Mattheolabakis, L. Milane, A. Singh, M.M. Amiji, Hyaluronic acid targeting of CD44 for cancer therapy: from receptor biology to nanomedicine, J. Drug Target. 23 (7–8) (2015) 605–618.
[40] M. Hanke-Roos, K. Fuchs, S. Maleschlijski, J. Sleeman, V. Orian-Rousseau, A. Rosenhahn, CD44 mediates the catch-bond activated rolling of HEPG2Iso epithelial cancer cells on hyaluronan, Cell Adhes. Migrat. 11 (5–6) (2017) 476–487.
[41] J. Kalia, R.T. Raines, Hydrolytic stability of hydrazones and oximes, Angew. Chem. 47 (39) (2008) 7523–7526.
[42] R. Patil, J. Portilla-Arias, H. Ding, B. Konda, A. Rekechenetskiy, S. Inoue, et al., Cellular delivery of doxorubicin via pH-controlled hydrazone linkage using multifunctional nano vehicle based on poly(β-l-malic acid), Int. J. Mol. Sci. 13 (9) (2012) 11681–11693.
[43] Z. Xu, K. Zhang, C. Hou, D. Wang, X. Liu, X. Guan, et al., A novel nanoassembled doxorubicin prodrug with a high drug loading for anticancer drug delivery, J. Mater. Chem. B 2 (22) (2014) 3433–3437.
[44] H. Tang, W. Zhao, J. Yu, Y. Li, C. Zhao, Recent development of pH-responsive polymers for cancer nanomedicine, Molecules 24 (1) (2018).
[45] M. Nejabat, M.R. Kalani, M. Nejabat, F. Hadizadeh, Dynamics, Molecular dynamic and in vitro evaluation of chitosan/tripolyphosphate nanoparticles as an insulin delivery system at two different pH values, J. Biomol. Struct. Dynam. 40 (20) (2022) 10153–10161.
[46] W. Gao, Z. Lin, M. Chen, X. Yang, Z. Cui, X. Zhang, et al., The co-delivery of a low-dose P-glycoprotein inhibitor with doxorubicin sterically stabilized liposomes against breast cancer with low P-glycoprotein expression, Int. J. Nanomed. 9 (2014) 3425–3437.
[47] Y. Xiao, H. Hong, V.Z. Matson, A. Javadi, W. Xu, Y. Yang, et al., Gold nanorods conjugated with doxorubicin and cRGD for combined anticancer drug delivery and PET imaging, Theranostics 2 (8) (2012) 757–768.
[48] M. Alibolandi, M. Ramezani, K. Abnous, F. Sadeghi, F. Atyabi, M. Asouri, et al., In vitro and in vivo evaluation of therapy targeting epithelial-cell adhesion-molecule aptamers for non-small cell lung cancer 209 (2015) 88–100.
[49] T. Zavvar, M. Babaei, K. Abnous, S.M. Taghdisi, S. Nekooei, M. Ramezani, et al., Synthesis of multimodal polymersomes for targeted drug delivery and MR/fluorescence imaging in metastatic breast cancer model 578 (2020) 119091.